

Accurate classification of 29 objects detected in the 39 month Palermo *Swift*/BAT hard X-ray catalogue^{★,★★}

P. Parisi^{1,4}, N. Masetti¹, E. Jiménez-Bailón², V. Chavushyan³, E. Palazzi¹, R. Landi¹, A. Malizia¹, L. Bassani¹, A. Bazzano⁴, A. J. Bird⁵, P. A. Charles¹⁰, G. Galaz⁶, E. Mason⁷, V. A. McBride^{10,11}, D. Minniti^{6,8}, L. Morelli⁹, F. Schiavone¹, and P. Ubertini⁴

¹ INAF – Istituto di Astrofisica Spaziale e Fisica Cosmica di Bologna, via Gobetti 101, 40129 Bologna, Italy
e-mail: pietro.parisi@iaps.inaf.it

² Instituto de Astronomía, Universidad Nacional Autónoma de México, Apartado Postal 70-264, 04510 México D.F., Mexico

³ Instituto Nacional de Astrofísica, Óptica y Electrónica, Apartado Postal 51-216, 72000 Puebla, Mexico

⁴ INAF – Istituto di Astrofisica e Planetologia Spaziali di Roma, via del Fosso del Cavaliere 100, 00133 Roma, Italy

⁵ Physics & Astronomy, University of Southampton, Southampton, Hampshire, SO171BJ, UK

⁶ Departamento de Astronomía y Astrofísica, Pontificia Universidad Católica de Chile, Casilla 306, Santiago 22, Chile

⁷ European Southern Observatory, Alonso de Cordova 3107, Vitacura, Santiago, Chile

⁸ Specola Vaticana, 00120 Città del Vaticano, Vatican

⁹ Dipartimento di Astronomia, Università di Padova, Vicolo dell'Osservatorio 3, 35122 Padua, Italy

¹⁰ South African Astronomical Observatory, PO Box 9, 7935 Observatory, South Africa

¹¹ University of Cape Town, Private Bag X3, 7701 Rondebosch, South Africa

Received 8 March 2012 / Accepted 15 June 2012

ABSTRACT

Through an optical campaign performed at four telescopes located in the northern and the southern hemispheres, plus archival data from two on-line sky surveys, we obtained optical spectroscopy for 29 counterparts of unclassified or poorly studied hard X-ray emitting objects detected with *Swift* /Burst Alert Telescope (BAT) and listed in the 39 month Palermo catalogue. All these objects also have observations taken with *Swift* /X-ray Telescope (XRT) or *XMM*-European Photon Imaging Camera (EPIC) which not only allow us to pinpoint their optical counterpart, but also study their X-ray spectral properties (column density, power law photon index, and F_{2-10} keV flux). We find that 28 sources in our sample are active galactic nuclei (AGNs); 7 are classified as type 1, while 21 are of type 2; the remaining object is a Galactic cataclysmic variable. Among our type 1 AGNs, we find 5 objects of intermediate Seyfert type (1.2–1.9) and one narrow-line Seyfert 1 galaxy; for 4 out of 7 sources, we are able to estimate the central black hole mass. Three of the type 2 AGNs of our sample display optical features typical of low-ionization nuclear emission-line regions (LINER) and one is a likely Compton thick AGN. All galaxies classified in this work are relatively nearby objects since their redshifts lie in the range 0.008–0.075; the only Galactic object found lies at an estimated distance of 90 pc. We also investigate the optical versus X-ray emission ratio of the galaxies of our sample to test the AGN unified model. For these galaxies, we also compare the X-ray absorption (caused by gas) with the optical reddening (caused by dust): we find that for most of our sources, specifically those of type 1.9–2.0 the former is higher than the latter confirming early results of Maiolino and collaborators; this is possibly due to the properties of dust in the circumnuclear obscuring torus of the AGN.

Key words. atomic data – X-rays: galaxies – X-rays: binaries – novae, cataclysmic variables

1. Introduction

A critically important region of the astrophysical spectrum is the hard X-ray band, from 15 keV to 200 keV, which has been explored in detail by the two satellites, INTEGRAL (Winkler et al. 2003) and *Swift* (Gehrels et al. 2004), which carry the instruments IBIS (Ubertini et al. 2003) and BAT (Barthelmy 2004) operating in the 20–200 keV band. These spacecrafts permit a

* Based on observations obtained from the following observatories: the Astronomical Observatory of Bologna in Loiano (Italy), ESO-La Silla Observatory (Chile) under programme 083.D-0110, Observatorio Astronómico Nacional (San Pedro Mártir, Mexico), and the South African Astronomical Observatory (South Africa).

** The spectra are only available at the CDS via anonymous ftp to [cdsarc.u-strasbg.fr](ftp://cdsarc.u-strasbg.fr) (130.79.128.5) or via <http://cdsarc.u-strasbg.fr/viz-bin/qcat?J/A+A/545/A101>

study of the processes taking place in this observational window providing a deep look into the physics of hard X-ray sources.

These telescopes operate in a complementary way, as the first concentrates on mapping the Galactic plane, while the second mainly covers the high Galactic latitude sky, so that together they provide the best sample of objects yet selected in the hard X-ray domain. So far, both instruments have detected a large number of both known and new objects, discovered new classes of sources, and allowed us to find and study highly absorbed objects. In particular, the nature of many objects detected above 20 keV by both satellites is often unknown, the sources being optically unclassified and their types only being able to be inferred based on few available X-ray or radio observations.

Optical follow-up of these sources is therefore mandatory. In particular, the optical spectra can provide not only an

accurate source classification, but also fundamental parameters that together with multiwaveband studies, for example in the soft X-ray band, can provide information on these newly detected objects.

In this paper, we focus on the X-ray and optical follow-up work of a number of objects with unknown classifications and/or redshifts, reported in the 39 month *Swift*/BAT survey catalogue (Cusumano et al. 2010a). We note that the identifications of the present paper are also reported in the Palermo 54 month catalogue (Cusumano et al. 2010b), and that preliminary classifications were given by us via private communication. Our aim is indeed to perform a systematic study of unidentified *Swift*/BAT objects starting with the 39 month surveys and continuing with the identifications of those of the 54 months catalogue (Parisi et al., in prep.).

This survey covers 90% of the sky down to a flux limit of 2.5×10^{-11} erg cm $^{-2}$ s $^{-1}$ and 50% of the sky down to a flux limit of 1.8×10^{-11} erg cm $^{-2}$ s $^{-1}$ in the 14–150 keV band. It lists 754 sources, of which 69% are extragalactic, 27% are galactic, and 4% are of unknown type.

From this BAT survey, we selected a sample of 29 objects either without optical identification, or that had not been well studied, or without published optical spectra. For all these sources, we first performed the X-ray data analysis to reduce the source positional uncertainty from arcmin-to arcsec-sized radii and derive information on the main spectral parameters (photon index, column density, and 2–10 keV flux). Within the reduced X-ray error boxes, we then identified the putative optical counterpart to the BAT object and performed optical spectroscopic follow-up work. Following the method applied by Masetti et al. (2004, 2006a,b, 2008, 2009, 2010, 2012) and Parisi et al. (2009), we determined the nature of all selected objects and discussed their properties. A preliminary classification of these sources was given in the Palermo 54 month BAT catalogue (Cusumano et al. 2010b), while here we publish for the first time the optical spectra and detailed optical information (see Tables 5–7).

We also checked for the presence of peculiar sources, such as Compton thick AGN, absorbed Seyfert 1's and unabsorbed Seyfert 2's, using the diagnostic method of Malizia et al. (2007), and finally used the plot of Maiolino et al. (2001) to verify a possible mismatch between the X-ray gas absorption and the optical dust reddening.

The paper is structured as follow: in Sect. 2, we report information on the soft X-ray data analysis; in Sect. 3, we describe the optical observations, the telescope employed, and provide information on the data reduction method used. Section 4 reports and discusses the main optical results (line fluxes, distances, Galactic and local extinction, central black hole masses etc.). In Sect. 5, the X-ray and the optical results are compared in view of the object classification and gas versus dust absorption. In Sect. 6, we summarize the main conclusions of our work.

2. X-ray data analysis

We now provide general information about the X-ray data analysis performed for the 29 objects of our sample, to obtain indications of the X-ray counterpart of the BAT object, provide its position with arcsec accuracy (see Table 1), and finally study its spectral properties in the 2–10 keV band (see Table 3).

For 24 of the 29 objects, we used X-ray data acquired with the X-ray Telescope (XRT, 0.3–10 keV, Burrows et al. 2004) onboard the *Swift* satellite. The XRT data reduction was performed using the XRTDAS standard data pipeline package (XRTPIPELINE v. 0.12.6), to produce screened event files. All

data were extracted in only the photon counting (PC) mode (Hill et al. 2004), adopting the standard grade filtering (0–12 for PC) according to the XRT nomenclature. Depending on the source nature (bright or dim), we either used the longest exposure or added multiple observations to enhance the signal-to-noise ratio (S/N). For each BAT detection, we then analysed, with XIMAGE v. 4.5.1, the 3–10 keV image of interest (single or added over more XRT pointings) to search for sources detected (at a confidence level $>3\sigma$) within the 90% *Swift*/BAT error circles; this 3–10 keV image choice ensured that we selected the hardest sources, hence the most likely counterparts to the BAT objects. We estimated the X-ray positions and relative uncertainties using the task XRTCENTROID v.0.2.9.

For 5 sources, we instead used X-ray data acquired with the pn X-ray CCD camera on the EPIC instrument onboard the *XMM-Newton* spacecraft (Strüder et al. 2001) in order to determine more reliably the spectral properties of those objects with low quality XRT data. These data were processed using the Standard Analysis Software (SAS) version 9.0.0 employing the latest available calibration files. Only patterns corresponding to single and double events (PATTERN ≤ 4) were taken into account and the standard selection filter FLAG = 0 was applied. For each source, we analysed a single observation, the longest in terms of exposure, to achieve higher quality statistics (see Table 2 for the observation (IDs)). In each case, we searched the *XMM-Newton* EPIC-pn images for X-ray sources that fell inside the *Swift*/BAT error circles; to avoid false associations with dim and soft objects, we only inspected higher energy (>4 keV) images in this case.

In 28 out of 29 objects analysed, a single object was detected within the BAT 90% positional uncertainty; the exception was PBC J0041.6+2534 for which we found one soft X-ray source located just outside the 90% error circle and none within it. Nevertheless, we consider it as the likely counterpart to the BAT source.

Next, we analysed the X-ray spectrum of each object. Events for spectral analysis were extracted within a circular region of radius 20'', centred on the source position for XRT¹ and choosing instead the radius corresponding to the highest Signal-to-Noise ratio for EPIC-pn. The background was taken from empty regions close to the X-ray source of interest, using circular regions with different radii for XRT data, to ensure an evenly sampled background. In the case of EPIC-pn, data we adopted instead an 80'' radius for all the 5 analysed sources. The XRT spectra were then extracted from the corresponding event files using the XSELECT v.2.4 software and binned using GRPPHA in an appropriate way, so that the χ^2 statistic could be applied. We used version v.011 of the response matrices and created the relative ancillary response file *arf* using the task XRTMKARF v.0.5.6.

For XMM spectra, ancillary response matrices (ARFs) and detector response matrices (RMFs) were generated using the *XMM-Newton* SAS tasks *arfgen* and *rmfgen*, respectively. In general, the spectral channels were rebinned to achieve a minimum of 20 counts in each bin (see however Table 3).

The energy band used for the spectral analysis, which was performed with XSPEC v.12.6.0, depends on the statistical quality of the data and typically ranges from 0.3 keV to ~6 keV for XRT and from 0.5 keV to 12 keV for EPIC-pn.

In the first instance, we adopted, as our basic model, a simple power-law passing through the Galactic (Dickey & Lockman 1990) and (when required) intrinsic absorption.

¹ This region encloses about 90% of the PSF at 1.5 keV (see Moretti et al. 2004).

Table 1. Log of the spectroscopic observations presented in this paper (see text for details).

(1) Object	(2) RA X-ray (J2000)	(3) Dec X-ray (J2000)	(4) Error radius (arcsec)	(5) RA Opt (arcsec)	(6) Dec Opt (arcsec)	(7) Telescope+instrument	(8) λ range (Å)	(9) Disp. (Å/pix)	(10) UT date & time at mid-exposure	(11) Exposure time (s)
PBC J0041.6+2534**	00 41 27.98	+25 29 57.78	4.59	00 41 28.01	+25 29 57.6	SPM 2.1 m+B&C Spc.	3450–7650	4.0	28 Jan. 2009, 03:18	2 × 1800
PBC J0100.6–4752	01 00 34.54	–47 52 05.71	3.75	01 00 34.90	–47 52 03.3	AAT+6dF	3900–7600	1.6	30 Oct. 2010, 14:34	1200+600
PBC J0122.3+5004	01 22 34.35	+50 03 12.24	4.59	01 22 34.42	+50 03 18.0	SPM 2.1 m+B&C Spc.	3450–7650	4.0	29 Jan. 2009, 03:48	2 × 1800
PBC J0140.4–5320	01 40 26.88	–53 19 37.28	3.62	01 40 26.78	–53 19 39.2	Radcliffe+Gr. Spec.	3850–7200	2.3	06 Aug. 2009, 02:46	2 × 900
PBC J0248.9+2627	02 48 59.17	+26 30 38.27	4.36	02 48 59.37	+26 30 39.1	SPM 2.1 m+B&C Spc.	3450–7650	4.0	02 Dec. 2008, 07:28	2 × 1800
PBC J0353.5+3713	03 53 42.28	+37 14 06.06	3.90	03 53 42.46	+37 14 07.7	SPM 2.1 m+B&C Spc.	3450–7650	4.0	28 Jan. 2009, 05:33	2 × 1800
PBC J0356.9–4040	03 56 56.40	–40 41 45.50	3.65	03 56 56.55	–40 41 45.3	AAT+6dF	3900–7600	1.6	19 Dec. 2003, 10:23	1200+600
PBC J0503.0+2300	05 02 58.10	+22 59 50.41	3.53	05 02 58.22	+22 59 52.0	SPM 2.1 m+B&C Spc.	3450–7650	4.0	28 Jan. 2009, 07:58	2 × 1800
PBC J0543.6–2738	05 43 33.07	–27 39 07.61	3.8	05 43 32.92	–27 39 05.3	SPM 2.1 m+B&C Spc.	3450–7650	4.0	02 Dec. 2008, 09:12	2 × 1800
PBC J0544.3+5905	05 44 22.29	+59 07 34.51	3.68	05 44 22.57	+59 07 36.1	SPM 2.1 m+B&C Spc.	3450–7650	4.0	03 Dec. 2008, 08:47	2 × 1800
PBC J0623.8–3212	06 23 46.37	–32 12 59.75	4.88	06 23 46.41	–32 12 59.9	AAT+6dF	3900–7600	1.6	07 Jan. 2002, 12:30	1200+600
PBC J0641.3+3251	06 41 18.00	+32 49 32.28	3.71	06 41 18.06	+32 49 31.3	Cassini+BFOSC	3500–8000	4.0	09 Dec. 2009, 20:43	2 × 1800
PBC J0759.9+2324	07 59 53.62	+23 23 23.29	3.79	07 59 53.47	+23 23 24.1	SDSS+CCD Spc.	3800–9200	1.0	09 Mar. 2003, 02:39	2220
PBC J0814.4+0421	08 14 25.22	+04 20 30.51	4.32	08 14 25.29	+04 20 32.4	SPM 2.1 m+B&C Spc.	3450–7650	4.0	28 Jan. 2009, 09:40	2 × 1800
PBC J0826.3–7033	08 26 23.19	–70 31 42.18	3.75	08 26 23.50	–70 31 43.1	NTT+EFOSC2	3650–9300	5.5	30 May 2009, 23:55	900
PBC J0919.9+3712*	09 19 57.90	+37 11 25.61	3.0	09 19 58.02	+37 11 27.7	SDSS+CCD Spc.	3800–9200	1.0	29 Nov. 2003, 10:11	2370
PBC J0954.8+3724	09 54 39.51	+37 24 30.84	4.64	09 54 39.43	+37 24 30.8	SDSS+CCD Spc.	3800–9200	1.0	25 Dec. 2003, 07:23	2250
PBC J1246.5+5432*	12 46 40.01	+54 31 59.77	5.08	12 46 39.82	+54 32 03.0	SPM 2.1 m+B&C Spc.	3450–7650	4.0	28 Jan. 2009, 11:49	2 × 1800
PBC J1335.8+0301*	13 35 48.44	+02 59 54.41	4.28	13 35 48.25	+02 59 55.6	SDSS+CCD Spc.	3800–9200	1.0	23 Apr. 2001, 06:07	7043
PBC J1344.2+1934	13 44 15.69	+19 33 59.61	6.41	13 44 15.80	+19 33 57.9	SPM 2.1 m+B&C Spc.	3450–7650	4.0	30 Jan. 2009, 04:45	2 × 1800
PBC J1345.4+4141	13 45 19.33	+41 42 45.15	4.28	13 45 19.13	+41 42 44.4	SDSS+CCD Spc.	3800–9200	1.0	15 Apr. 2004, 08:41	2400
PBC J1439.0+1413	14 39 11.87	+14 15 18.46	3.91	14 39 11.86	+14 15 21.5	SPM 2.1 m+B&C Spc.	3450–7650	4.0	01 Feb. 2009, 12:52	2 × 1800
PBC J1453.0+2553	14 53 07.66	+25 54 33.99	3.55	14 53 07.91	+25 54 33.2	SPM 2.1 m+B&C Spc.	3450–7650	4.0	31 Jan. 2009, 11:48	1800+1200
PBC J1506.6+0349	15 06 43.95	+03 51 45.43	3.68	15 06 44.12	+03 51 44.4	SPM 2.1 m+B&C Spc.	3450–7650	4.0	01 Feb. 2009, 10:48	2 × 1800
PBC J1546.5+6931	15 46 23.85	+69 29 10.74	4.55	15 46 24.24	+69 29 10.2	Cassini+BFOSC	3500–8000	4.0	18 May 2009, 22:06	2 × 1800
PBC J1620.3+8101	16 19 19.94	+81 02 46.30	3.74	16 19 19.31	+81 02 47.3	Cassini+BFOSC	3500–8000	4.0	15 May 2009, 23:34	1800
PBC J2148.2–3455	21 48 19.21	–34 57 02.77	5.24	21 48 19.48	–34 57 04.7	AAT+6dF	3900–7600	1.6	07 Jul. 2003, 16:40	1200+600
PBC J2333.9–2343	23 33 55.25	–23 43 41.76	3.54	23 33 55.20	–23 43 40.6	SPM 2.1 m+B&C Spc.	3450–7650	4.0	18 Sep. 2009, 07:48	2 × 1800
PBC J2341.9+3036*	23 41 55.25	+30 34 53.97	4.45	23 41 55.45	+30 34 54.2	SPM 2.1 m+B&C Spc.	3450–7650	4.0	02 Dec. 2008, 03:10	2 × 1800

Notes. Optical source coordinates are extracted from the 2MASS catalogue and have an accuracy better than $0''.1$, and soft X-ray coordinates are extracted from XRT and *XMM-Newton* observations. If not indicated otherwise, source optical coordinates were extracted from the 2MASS catalogue and have an accuracy better than $0''.1$. (*) The reported X-ray coordinates are obtained from XMM/EPIC data. Our positions totally agree with those in the 2XMM catalogue (Watson et al. 2009). (+) This source is outside the BAT 90% error box, but within the 99% one.

Table 2. Observation IDs of the *XMM-Newton* sources presented in this paper.

Object	Observation IDs
PBC J0041.6+2534	0153030101
PBC J0919.9+3712	0149010201
PBC J1246.9+5432	0554500101
PBC J1335.8+0301	0601781201
PBC J2341.9+3036	0554500501

If this baseline model was insufficient to fit the data, we introduced additional spectral components (i.e. a black body, second-power law, or Gaussian line) as required according to the F-test statistics.

We note that in some cases owing to the limited statistical quality of the XRT data we fixed the photon index to 1.8 (which is the canonical value for AGN; e.g., Mushotzky et al. 1993) to estimate the intrinsic column density and/or the X-ray flux.

We are aware that in a few cases the statistical quality of the data is such that the obtained parameter values must be interpreted with caution. Nevertheless, they provide some indications of the source properties, i.e. whether a source is likely to be absorbed or not.

The results of the X-ray spectral analysis are reported in Table 3, where we list for each object the Galactic column density, the power-law photon index, the column density in excess to the Galactic value, the reduced χ^2 of the best-fit model, the 2–10 keV flux, and the 20–100 keV flux² additional spectral parameters, if they were required, are reported in the notes at the end of the table. Here and in the following all quoted errors correspond to a 90% confidence level for a single X-ray parameter of interest ($\Delta\chi^2 = 2.71$).

We note that for a limited number of our sources, X-ray data were previously published. Winter et al. (2009) discuss the spectra of PBC J0641.3+3251 and PBC J0356.9-4040 while Noguchi et al. (2009) analysed the *XMM-Newton* of PBC J0919.9+3712. Finally, PBC J2148.2-3455 has been extensively studied at X-ray energies using various instruments, such as *XMM-Newton* and Chandra (see for example González-Martín et al. 2009; Levenson et al. 2005), but no XRT data have been yet presented. Overall, we find good agreement with these previous studies.

3. Optical spectroscopy

We describe the optical follow-up studies that we performed for all 29 objects. We list in Table 1 the coordinates of the optical counterparts obtained from the 2MASS catalogue³ (Skrutskie et al. 2006). In all but one case, these optical counterparts coincide in position with a galaxy, which immediately suggests that the majority of the objects listed in Table 1 are active galaxies (their name as derived by NED⁴ is reported in Tables 6 and 7). The only exception is PBC J0826.3-7033, which is listed in NED and SIMBAD⁵ as an unidentified X-ray source; our optical follow-up study located this source at $z = 0$, thus demonstrates that it is not an extragalactic object but rather a Galactic high-energy source.

Of the 28 AGN, 10 objects already have a known redshift, although these are not supported by published optical spectra, 9 have redshifts obtained from the Sloan Digital Sky Survey⁶ (SDSS, Adelman-McCarthy et al. 2007) and the Six-degree Field Galaxy Survey (6dFGS; Jones et al. 2004) archives and 9 have redshifts that were derived from our spectroscopic observations and therefore published here for the first time. In one case (a 6dF spectrum), our result differs significantly from the one reported in the literature (see Sect. 4), suggesting that it is important to confirm published redshift values especially for newly discovered objects.

Concerning the optical classes for all our sample, 12 objects had an optical class that had already been reported in the Veron-Chetty & Veron 13th catalogue edition (V&V13, Veron-Chetty & Veron 2010 and references therein) and/or in NASA/IPAC extragalactic database (NED). Nevertheless, we chose to report data on these 12 sources for a number of reasons: in a few cases, our classification is different or more detailed than the one reported in the literature, and for a couple of sources different authors provide contradictory results, thus the classification is ambiguous. For the remaining 17 objects, we reported the optical class supported by optical spectra for the first time.

In Table 1, the detailed log of all optical measurements is also reported: we list in Col. 7 the telescope and instrument used for the observation, while the characteristics of each spectrograph are given in Cols. 8 and 9. Column 10 provides the observation date and the UT time at mid-exposure, while Col. 11 reports the exposure times and the number of spectral pointings.

For 20 sources, the following telescopes were used for the optical spectroscopic study presented here:

- the 1.52 m “Cassini” telescope of the Astronomical Observatory of Bologna, in Loiano, Italy;
- the 1.9 m “Radcliffe” telescope of the South African Astronomical Observatory (SAAO) in Sutherland, South Africa;
- the 2.1 m telescope of the Observatorio Astrónomico Nacional in San Pedro Martir, Mexico;
- the 3.58 m New Technology Telescope (NTT) at the ESO-La Silla Observatory, Chile.

The data reduction was performed with the standard procedure (optimal extraction, Horne 1986) using IRAF⁷. Calibration frames (flat fields and bias) were taken on the day preceding or following the observing night. The wavelength calibration was obtained using lamp spectra acquired soon after each on-target spectroscopic acquisition. The uncertainty in the calibration was ~ 0.5 Å in all cases; this was checked using the positions of background night-sky lines. Flux calibration was performed using catalogued spectrophotometric standards. Objects with more than one observation had their spectra stacked together to increase the S/N.

Additional spectra (that is, 9 out of 29) were retrieved from two different astronomical archives: the SDSS and the 6dFGS⁸. As the 6dFGS archive provides spectra that have not been flux calibrated, we used the optical photometric information in Jones

⁶ <http://www.sdss.org>

⁷ IRAF is the Image Reduction and Analysis Facility made available to the astronomical community by the National Optical Astronomy Observatories, which are operated by AURA, Inc., under contract with the US National Science Foundation. It is available at <http://iraf.noao.edu/>

⁸ <http://www.aao.gov.au/local/www/6df/>

² Hard X-ray fluxes were extrapolated from 15–150 keV fluxes assuming a power law with $\Gamma = 2.02$ (see Molina et al., in prep.).

³ Available at <http://www.ipac.caltech.edu/2mass/>

⁴ <http://ned.ipac.caltech.edu/>

⁵ <http://simbad.u-strasbg.fr/simbad/>

Table 3. Main results obtained from the analysis of the X-ray spectra of all AGN present in the sample.

Source	N_{Hgal} $\times 10^{22} \text{ cm}^{-2}$	Γ^+	N_{H} $\times 10^{22} \text{ cm}^{-2}$	χ^2/ν	$F_{(2-10) \text{ keV}}$ $\times 10^{-11} \text{ erg s}^{-1} \text{ cm}^{-2}$	$F_{(20-100) \text{ keV}}$ $\times 10^{-11} \text{ erg s}^{-1} \text{ cm}^{-2}$
PBC J0041.6+2534^A	0.038	2.56^{+0.31}_{-0.21}	21.2^{+11.4}_{-7.8}	6.2/7	0.02	1.0
PBC J0100.6–4752 ^A	0.019	1.67 ^{+0.37} _{-0.54}	4.5 ^{+1.8} _{-1.6}	4.3/11	0.28	0.6
PBC J0122.3+5004 ^A	0.136	2.22 ^{+0.70} _{-0.60}	44 ⁺¹²⁹ ₋₃₅	1.9/3	0.09	0.6
PBC J0140.4–5320 ^A	0.026	1.58 ^{+0.25} _{-0.23}	1.2 ^{+0.4} _{-0.3}	28.7/26	0.50	0.7
PBC J0248.9+2627	0.103	[1.8]	41.2 ^{+20.8} _{-14.2}	3.6/3	0.40	1.2
PBC J0353.5+3713 ^A	0.168	1.71 ^{+0.59} _{-0.55}	3.7 ^{+2.0} _{-1.7}	13.2/14	0.35	0.8
PBC J0356.9–4040 ^A	0.019	1.83 ^{+0.16} _{-0.31}	4.0 ^{+0.9} _{-0.9}	25.9/38	0.74	1.1
PBC J0503.0+2300	0.226	2.11 ^{+0.08} _{-0.08}	0.11 ^{+0.03} _{-0.02}	148.6/149	1.25	1.1
PBC J0543.6–2738 ^A	0.022	2.38 ^{+0.46} _{-0.50}	3.6 ^{+1.9} _{-1.2}	8.3/8	0.47	1.1
PBC J0544.3+5905	0.158	1.22 ^{+0.44} _{-0.29}	1.5 ^{+0.7} _{-0.4}	8.3/18	0.47	1.1
PBC J0623.8–3212 ^B	0.038	[1.8]	43.9 ^{+15.8} _{-8.7}	3.3/2	0.07	1.5
PBC J0641.3+3251 ^A	0.159	1.72 ^{+0.32} _{-0.21}	12.2 ^{+4.2} _{-3.7}	14.5/16	0.29	1.0
PBC J0759.9+2324	0.047	1.57 ^{+0.56} _{-0.49}	1.6 ^{+0.9} _{-0.5}	9/10	0.44	1.3
PBC J0814.4+0421	0.032	1.2 ^{+0.80} _{-0.65}	5.6 ^{+2.9} _{-2.0}	9.3/15	0.50	1.1
PBC J0919.9+3712^{C1}	0.011	1.66^{+0.07}_{-0.07}	7.2^{+0.4}_{-0.4}	326.9/328	0.36	1.2
PBC J0954.8+3724 [*]	0.014	[1.8]	21.4 ^{+13.8} _{-8.3}	2.4/2	0.15	0.4
PBC J1246.9+5432^D	0.014	0.88^{+0.13}_{-0.12}	23.6^{+8.0}_{-9.6}	15/22	0.09	1.5
PBC J1335.8+0301^A	0.019	1.58^{+0.06}_{-0.04}	2.3^{+0.1}_{-0.1}	313.3/299	0.64	1.1
PBC J1344.2+1934	0.017	[1.8]	38 ⁺⁵⁶ ₋₂₀	2/4	0.10	0.9
PBC J1345.4+4141 ^A	0.009	1.38 ^{+0.27} _{-0.25}	0.8 ^{+0.4} _{-0.3}	10.4/25	0.74	0.7
PBC J1439.0+1413 ^A	0.014	[1.8]	3.4 ^{+1.1} _{-1.0}	12/8	0.32	0.5
PBC J1453.0+2553	0.033	1.72 ^{+0.05} _{-0.05}	–	73.8/87	1.06	1.0
PBC J1506.6+0349	0.037	1.36 ^{+0.35} _{-0.28}	1.1 ^{+0.4} _{-0.3}	14/19	0.42	0.7
PBC J1546.5+6931 [*]	0.031	[1.8]	16 ⁺²⁶ _{-8.0}	3.3/2	0.08	0.5
PBC J1620.3+8101	0.046	[1.8]	10.1 ^{+2.1} _{-1.6}	9.6/13	0.54	0.7
PBC J2148.2–3455	0.019	[1.8]	–	6/11	0.04	0.9
PBC J2333.9–2343	0.016	1.67 ^{+0.04} _{-0.04}	–	97/104	0.80	0.7
PBC J2341.9+3036^{C2}	0.058	2.02^{+0.16}_{-0.15}	56.5^{+15.5}_{-10.4}	25/28	0.11	1.0

Notes. ⁽⁺⁾ The square brackets in the Γ column indicate that we used a fixed value. ^(*) Grouping of 10 instead of 20 applied owing to the poor statistical quality of the data. ^(A) Best-fit model requires an extra power-law component, having the same photon index as the primary absorbed power-law and passing only through the galactic column density ($\text{wa}_{\text{gal}}^*(\text{po}+\text{wa}^*\text{po})$ in xspec terminology). ^(B) Best-fit model requires an extra black-body component with $kT = 0.16^{+0.04}_{-0.03}$ keV ($\text{wa}_{\text{gal}}^*(\text{bb}+\text{wa}^*\text{po})$ in xspec terminology). ^(C1) Best-fit model requires an extra power-law component, having the same photon index as the primary absorbed power-law and passing only through the Galactic column density plus a narrow line at $E = 6.36^{+0.03}_{-0.03}$ keV with $EW = 194^{+20}_{-42}$ eV ($\text{wa}_{\text{gal}}^*(\text{po}+\text{wa}^*(\text{po}+\text{ga}))$ in xspec terminology). ^(D) Best-fit model requires a black-body component with a $kT = 0.28^{+0.04}_{-0.03}$ keV and two narrow lines at $E = 6.29^{+0.03}_{-0.03}$ keV and $6.79^{+0.11}_{-0.10}$ keV with an EW of 600^{+182}_{-174} eV and 378^{+168}_{-167} eV, respectively ($\text{wa}_{\text{gal}}^*(\text{bb}+\text{wa}^*(\text{po}+\text{ga}+\text{ga}))$ in xspec terminology). ^(C2) Best-fit model requires a second power-law component, having the same photon index as the primary absorbed power-law and passing only through the Galactic column density plus a narrow line with $E = 6.25^{+0.05}_{-0.06}$ and 365^{+176}_{-147} eV ($\text{wa}_{\text{gal}}^*(\text{po}+\text{wa}^*(\text{po}+\text{ga}))$ in xspec terminology).

In bold face, we indicate sources for which we performed an X-ray data analysis using *XMM-Newton* observations.

Table 4. Main X-ray results for PBC J0826.3–7033.

Source	N_{Hgal} $\times 10^{22} \text{ cm}^{-2}$	kT keV	χ^2/ν	$F_{(2-10) \text{ keV}}$ $\times 10^{-11} \text{ erg s}^{-1} \text{ cm}^{-2}$	$F_{(20-100) \text{ keV}}$ $\times 10^{-11} \text{ erg s}^{-1} \text{ cm}^{-2}$
PBC J0826.3–7033	0.06 ± 0.06	$3.3^{+1.9}_{-1.0}$	14.5/11	0.2	0.8

Table 5. Main optical results concerning PBC J0826.3–7033, which was identified as a cataclysmic variable.

Object	H_α		H_β		He II $\lambda 4686$		Optical mag	A_V (mag)	d (pc)	L_X
	EW	Flux	EW	Flux	EW	Flux				
PBC J0826.3–7033	38.9 ± 1.8	66 ± 3	33.6 ± 1.5	44 ± 2	5.7 ± 0.9	7.4 ± 1.1	13.8 (R)	0	90	2 (2–10) 7(20–100)

Notes. EWs are expressed in Å, line fluxes are in units of 10^{-15} erg cm $^{-2}$ s $^{-1}$, and X-ray luminosities are in units of 10^{30} erg s $^{-1}$.

Table 6. Main results obtained from the analysis of the optical spectra of the 7 type 1 AGNs.

Object	$F_{H_\alpha}^*$	F_{H_β}	$F_{[OIII]}$	Class	z	D_L (Mpc)	$E(B - V)$		NED name
							Gal.	AGN	
PBC J0503.0+2300	699 ± 55 [2670 ± 153]	113 ± 23 [600 ± 64]	93 ± 7 [436 ± 45]	Sy1.5	0.058	259.3	0.515	0.424	2MASX J05025822+2259520
PBC J0543.6–2738	83.9 ± 18.4 [88 ± 14.9]	107 ± 17 [120 ± 9]	22.6 ± 3.1 [25.4 ± 3.2]	Sy1.2	0.009	38.8	0.029	0	ESO 424-G012
PBC J0814.4+0421	394 ± 35 [433 ± 37]	43.9 ± 7.7 [49.5 ± 7.8]	31.9 ± 2.3 [36.3 ± 5.6]	NLS1	0.034	149.4	0.027	1.073	CGCG 031-072
PBC J1345.4+4141	27.3 ± 1.5 [33.9 ± 1.9]	0.7 ± 0.2 [0.7 ± 0.2]	3.7 ± 1.8 [3.7 ± 1.8]	Sy1.9	0.009	37.1	0.007	2.716	NGC 5290
PBC J1439.0+1413	16.5 ± 3.1 [17.7 ± 3.2]	–	–	Sy1.9	0.072	325.1	0.019	–	2MASX J14391186+1415215
PBC J1453.0+2553	470 ± 68 [502 ± 72]	111 ± 22 [115 ± 22]	19.7 ± 3.3 [20.6 ± 3.3]	Sy1	0.049	217.7	0.039	0.406	2MASX J14530794+2554327
PBC J1546.5+6931	181 ± 20 [244 ± 23]	26 ± 5 [29 ± 5]	97.8 ± 8.6 [113 ± 16]	Sy1.9	0.037	162.9	0.041	1.036	2MASX J15462424+6929102

Notes. Emission line fluxes are reported both as observed and (between square brackets) corrected for the intervening Galactic absorption $E(B - V)_{Gal}$ along the object line of sight (from Schlegel et al. 1998). Line fluxes are in units of 10^{-15} erg cm $^{-2}$ s $^{-1}$, the typical error on the redshift measurement is ± 0.001 except for the SDSS and 6dFGS spectra, for which an uncertainty of ± 0.0003 can be assumed. (*) Blended with [N II] lines.

et al. (2005) and Doyle et al. (2005) to calibrate the 6dFGS data presented here.

The identification and classification approach we adopt in the analysis of the optical spectra is the following: for the emission-line AGN classification, we used the criteria of Veilleux & Osterbrock (1987) and the line-ratio diagnostics of Ho et al. (1993, 1997) and Kauffmann et al. (2003) to distinguish among the Seyfert 2, starburst galaxies, HII regions, and low-ionization nuclear emission-line regions (LINERs; Heckman 1980). In this last class, some lines ([OII] λ_{3723} , [OI] λ_{6300} , and [NII] λ_{6584}) are stronger than in typical Seyfert 2 galaxies; the permitted emission-line luminosities are weak; and the emission-line widths are comparable with those of type 2 AGNs. In particular, as mentioned in Ho et al. (1993), all sources with [OII] > [OIII], [NII]/ H_α > 0.6, [OI] > 1/3 [OIII] can be considered LINERs (see Table 7). For the subclass assignment to Seyfert 1 galaxies, we used the H_β /[O III] λ_{5007} line flux ratio criterion presented in Winkler et al. (1992). Moreover, the criteria of Osterbrock & Pogge (1985) allowed us to discriminate between “normal” Seyfert 1 and narrow-line Seyfert 1 (NLS1): the latter are galaxies with a full width at half-maximum (FWHM) of the H_β line lower than 2000 km s $^{-1}$, with permitted

lines which are only slightly broader than their forbidden lines, with a [OIII] λ_{5007} / H_β ratio < 3, and finally with evident FeII and other high-ionization emission-line complexes.

We note that the spectra of all extragalactic objects are not corrected for starlight contamination (see, e.g., Ho et al. 1993, 1997), because of their limited S/N and spectral resolution. However, this does not affect our results and conclusions.

To estimate the $E(B - V)$ local optical absorption in our AGN sample, when possible, we first dereddened the H_α and H_β line fluxes by applying a correction for the Galactic absorption along the line of sight to the source. This was done using the galactic colour excess $E(B - V)_{Gal}$ given by Schlegel et al. (1998) and the Galactic extinction law obtained by Cardelli et al. (1989). We then estimated the colour excess $E(B - V)_{AGN}$ local to the AGN host galaxy by comparing the intrinsic line ratio and corrected that for Galactic reddening using the relation for type 2 AGNs derived from Osterbrock (1989)

$$E(B - V) = a \text{Log} \left(\frac{H_\alpha/H_\beta}{(H_\alpha/H_\beta)_0} \right).$$

For type 1 objects, where the H_α is strongly blended with the forbidden narrow [NII] lines, it is not easy to obtain a reliable

Table 7. Main results obtained from the analysis of the optical spectra of the 21 type 2 AGN.

Object	$F_{H\alpha}$	$F_{H\beta}$	$F_{[OIII]}$	Class	z	D_L (Mpc)	$E(B - V)$		NED name
							Gal.	AGN	
PBC J0041.6+2534	11.3 ± 4.5 [12.1 ± 3.8]	–	–	Sy2/LINER	0.015	65.0	0.035	–	NGC 214
PBC J0100.6–4752	37 ± 4 [38 ± 4]	10.8 ± 2.9 [12.6 ± 3]	101 ± 6 [106 ± 6]	Sy2	0.048	213.1	0.013	0.051	ESO 195-IG021
PBC J0122.3+5004	139 ± 23 [188 ± 31]	34.1 ± 5.7 [55 ± 9]	169 ± 28 [270 ± 50]	Sy2	0.021	91.4	0.217	0.171	MCG +08-03-018
PBC J0140.4–5320	27.3 ± 4.3 [31.6 ± 4.8]	4.6 ± 0.9 [5.4 ± 0.9]	39.1 ± 1.3 [42.7 ± 1.4]	Sy2	0.072	325.1	0.029	0.687	2MASX J01402676-5319389
PBC J0248.9+2627	47 ± 4 [64.3 ± 15.7]	4.2 ± 0.5 [6.3 ± 0.9]	21.6 ± 1.5 [34.4 ± 2.5]	Sy2	0.057	274.3	0.158	1.221	2MASX J02485937+2630391
PBC J0353.5+3713	35.5 ± 2.8 [120 ± 13]	6 ± 1 [37.6 ± 6.4]	12.8 ± 1.3 [71.4 ± 13.9]	LINER	0.019	82.6	0.536	0.105	2MASX J03534246+3714077
PBC J0356.9–4040	75.6 ± 11.8 [70.1 ± 7.2]	21.7 ± 5.6 [22.4 ± 5.6]	167 ± 9 [170 ± 9]	Sy2	0.075	65.0	0.035	0.086	2MASX J03565655-4041453
PBC J0544.3+5905	3.9 ± 0.5 [6.4 ± 0.8]	0.7 ± 0.1 [1.4 ± 0.2]	7.1 ± 0.4 [15.9 ± 0.8]	Sy2	0.068	306.2	0.274	0.451	2MASX J05442257+5907361
PBC J0623.8–3212	97.9 ± 17.4 [112 ± 13.6]	–	783 ± 40 [908 ± 47]	Sy2	0.035	153.9	0.049	–	ESO 426-G002
PBC J0641.3+3251	51.9 ± 6.4 [69.4 ± 10.4]	8.2 ± 1.7 [13.3 ± 2.1]	197 ± 6.2 [311 ± 20]	Sy2	0.049	217.7	0.153	0.577	2MASX J06411806+3249313
PBC J0759.9+2324	8.9 ± 1.1 [9.8 ± 1.1]	1.1 ± 0.3 [1.4 ± 0.4]	10.6 ± 1.1 [13.5 ± 1.2]	Sy2	0.029	127	0.059	0.859	CGCG 118-036
PBC J0919.9+3712	4.3 ± 0.4 [4.4 ± 0.4]	0.5 ± 0.1 [0.5 ± 0.1]	4.1 ± 0.3 [4.2 ± 0.3]	Sy2	0.0075	32.3	0.012	1.079	IC 2461
PBC J0954.8+3724	8.6 ± 0.5 [8.8 ± 0.6]	0.8 ± 0.03 [0.8 ± 0.2]	3.6 ± 0.6 [3.7 ± 0.5]	Sy2	0.019	82.6	0.016	1.292	IC 2515
PBC J1246.9+5432	–	–	16.4 ± 4.2 [17.8 ± 4.4]	Sy2	0.017	73.8	0.017	–	NGC 4686
PBC J1335.8+0301	19.6 ± 2.4 [20.7 ± 1.9]	2.9 ± 0.5 [3.2 ± 0.5]	16.9 ± 1.3 [17.9 ± 1.1]	Sy2	0.0218	94.9	0.024	1.014	NGC 5231
PBC J1344.2+1934	16.6 ± 1.8 [17.2 ± 1.8]	–	6.6 ± 1.1 [6.9 ± 1.2]	Sy2/LINER	0.027	118	0.027	–	CGCG 102-048
PBC J1506.6+0349	17.2 ± 1.1 [19.4 ± 2.6]	2.5 ± 0.6 [2.7 ± 0.7]	20.8 ± 0.8 [23.7 ± 1.4]	Sy2	0.038	167.5	0.049	0.884	2MASX J15064412+0351444
PBC J1620.3+8101	2.4 ± 0.8 [27.9 ± 7.8]	2.5 ± 0.6 [4.1 ± 1.5]	19.2 ± 3.9 [23.9 ± 4.5]	Sy2	0.025	109.1	0.046	0.832	CGCG 367-009
PBC J2148.2–3455	6460 ± 582 [6900 ± 895]	857 ± 83 [947 ± 117]	4970 ± 347 [5440 ± 347]	Sy2	0.0161	70.7	0.029	0.832	NGC 7130
PBC J2333.9–2343	–	3.2 ± 1.2 [3.5 ± 1.2]	14.7 ± 2.8 [16.3 ± 2.8]	Sy2	0.0475	210.8	0.029	–	PKS 2331-240
PBC J2341.9+3036	9.7 ± 4.6 [14.2 ± 5.3]	–	8.3 ± 2.1 [15.6 ± 2.9]	Sy2	0.017	73.8	0.102	–	UGC 12741

Notes. Emission line fluxes are reported both as observed and (between square brackets) corrected for the intervening Galactic absorption $E(B - V)_{\text{Gal}}$ along the object line of sight (from Schlegel et al. 1998). Line fluxes are in units of 10^{-15} erg cm $^{-2}$ s $^{-1}$, the typical error on the redshift measurement is ± 0.001 except for the SDSS and 6dFGS spectra, for which an uncertainty of ± 0.0003 can be assumed.

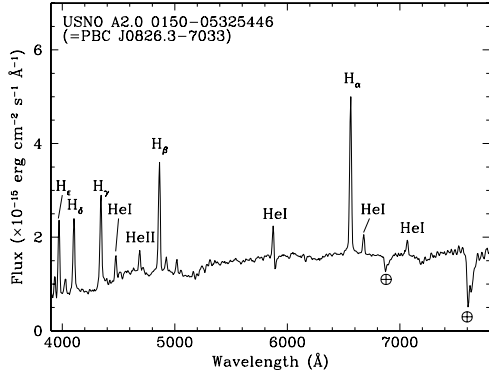


Fig. 1. Spectrum (uncorrected for the intervening Galactic absorption) of the optical counterpart of the Galactic CV PBC J0826.3-7033.

Table 8. Broad-line region gas velocities and central black hole masses for 4 Seyfert 1 AGNs listed in this paper.

Object	v_{BLR} (km s ⁻¹)	M_{BH} (10 ⁷ M _⊙)
PBC J0503.0+2300	3600	5.2
PBC J0543.6-2738	4500	7.1
PBC J0814.4+0421	1800	1.1
PBC J1453.0+2553	10 800	43

H_{α}/H_{β} estimate. In these cases, we used the H_{γ}/H_{β} ratio, taking into account that H_{γ} may also be blended with the [O III]_{λ4363} line. In the above relation, H_{α}/H_{β} is the observed Balmer decrement, $(H_{\alpha}/H_{\beta})_0$ is the intrinsic one (2.86), and a is a constant with a value of 2.21. When instead we used the H_{γ} , we adopted the same relation described before, using an intrinsic $(H_{\gamma}/H_{\beta})_0$ of 0.474 with an a value of -5.17 .

Finally, we estimated the mass of the central black hole for a few type 1 AGN found in the sample⁹. The method used here follows the prescription of Wu et al. (2004) and Kaspi et al. (2000), where we used the H_{β} emission line flux, corrected for the Galactic colour excess (Schlegel et al. 1998), and the broad-line region (BLR) gas velocity (v_{FWHM}). Using Eq. (2) of Wu et al. (2004), we estimated the BLR size, which is used with v_{FWHM} in Eq. (5) of Kaspi et al. (2000) to calculate the AGN black hole mass. The results are reported in Table 8.

To derive the distance of the only compact Galactic X-ray source of our sample, we used the distance modulus assuming an absolute magnitude $M_V \sim +9$ and an intrinsic colour index $(V - R)_0 \sim 0$ mag (Warner 1995). Although this method basically provides an order-of-magnitude value for the distance of this Galactic source, our past experience (Masetti et al. 2004, 2006a,b, 2008, 2009, 2010) tells us that this estimate is in general correct to within 50% of the refined value subsequently determined with more precise approaches. To calculate instead the luminosity distances of the 28 galaxies in the sample, we considered a cosmology with $h_0 = 70$ km s⁻¹ Mpc⁻¹, $\Omega_{\Lambda} = 0.7$, and $\Omega_m = 0.3$ and used the Cosmology Calculator of Wright (2006).

4. Optical classification

We discuss the optical classifications found and highlight the most interesting or peculiar objects discovered. The

⁹ We could not estimate the mass of the central black hole of PBC J1439.0+1413 because it lacks the H_{β} emission line, and for PBC J1345.4+4141 and PBC J1546.5+6931 only because the narrow component of the H_{β} line was observed in their spectra.

B magnitudes if not otherwise stated, are extracted from the Linked Extragalactic Database and Archives (LEDA, Prugniel et al. 2005) and the R magnitudes from the USNO-A2.0 catalogue (The United States Naval Observatory, Monet et al. 2003).

4.1. Galactic object

PBC J0826.3-7033 is the only source that displays emission lines of the Balmer complex (up to at least H_{ϵ}), as well as He I and He II, consistent with $z = 0$, indicating that this object lies within our Galaxy (see Fig. 1). The analysis of all these optical features indicates that this source is a cataclysmic variable (CV, see Table 1). The $\text{He II}_{\lambda 4686}/H_{\beta}$ equivalent width (EW) ratio, which is smaller than 0.5, and the EW of these two emission lines (only the H_{β} EW is larger than 10 Å) point out that this source is likely a non-magnetic CV (see Warner 1995, and references therein). The H_{α} to H_{β} flux ratio is ~ 1.5 allowing us to assume that the absorption along the line of sight is negligible. This is in line with the hydrogen column density value obtained from the X-ray spectral analysis (see below). The source was previously detected at soft X-ray energies, being listed for example in the Rosat Bright source catalogue (Voges et al. 1999); as for many other CVs, PBC J0826.3-7033 is also located at relatively high Galactic latitudes, i.e. 18 degrees above the Galactic plane.

We also estimated its distance to be 90 pc, i.e. relatively close, assuming no Galactic extinction along the line of sight. The X-ray spectrum is best fitted with a bremsstrahlung model (see Table 4 for more information). At the estimated distance, the 2-10 keV source luminosity is around 2×10^{30} erg s⁻¹, which is relatively low compared to the CVs so far detected in hard X-rays (Landi et al. 2009). Finally, we estimated the mass of the white dwarf using Eqs. (5) and (6) of Patterson & Raymond (1985). Using the bremsstrahlung temperature of our model (see Table 4) and a 0.2-4 keV luminosity of $\sim 2.5 \times 10^{30}$ erg s⁻¹, we obtained a value of about $0.4 M_{\odot}$.

4.2. Extragalactic objects

The results of our optical study of extragalactic sources are reported in Tables 6 and 7, where for each source we list the H_{α} , H_{β} , and [OIII] fluxes, the classification, the redshift estimated from the narrow lines, the luminosity distance given in Mpc, the Galactic colour excess and the colour excess local to the AGN host. All the extragalactic optical spectra are displayed in Figs. 2 and 3. Of the 28 active galaxies found, 7 have strong redshifted broad and narrow emission-lines that are typical of Seyfert 1 galaxies, while the remaining 21 display only the strong and redshifted narrow emission-lines typical of Seyfert 2 galaxies (for the subclass classification see Tables 6 and 7). As reported before, some sources have a preliminary classification and/or redshift in the Palermo 54 month BAT catalogue (Cusumano et al. 2010b), while here we publish for the first time their optical spectra and the corresponding information.

4.2.1. Redshifts

We confirm the redshift estimates reported in NED, V&V13, and Ciroi et al. (2009) for 19 AGN. In one case (PBC J0623.8-3212), we obtain a different redshift (0.035) from the one (0.022) already available, despite both redshifts being extracted from the same 6dF spectrum. The origin of this discrepancy is unclear. For the remaining 9 sources, we report the redshifts derived

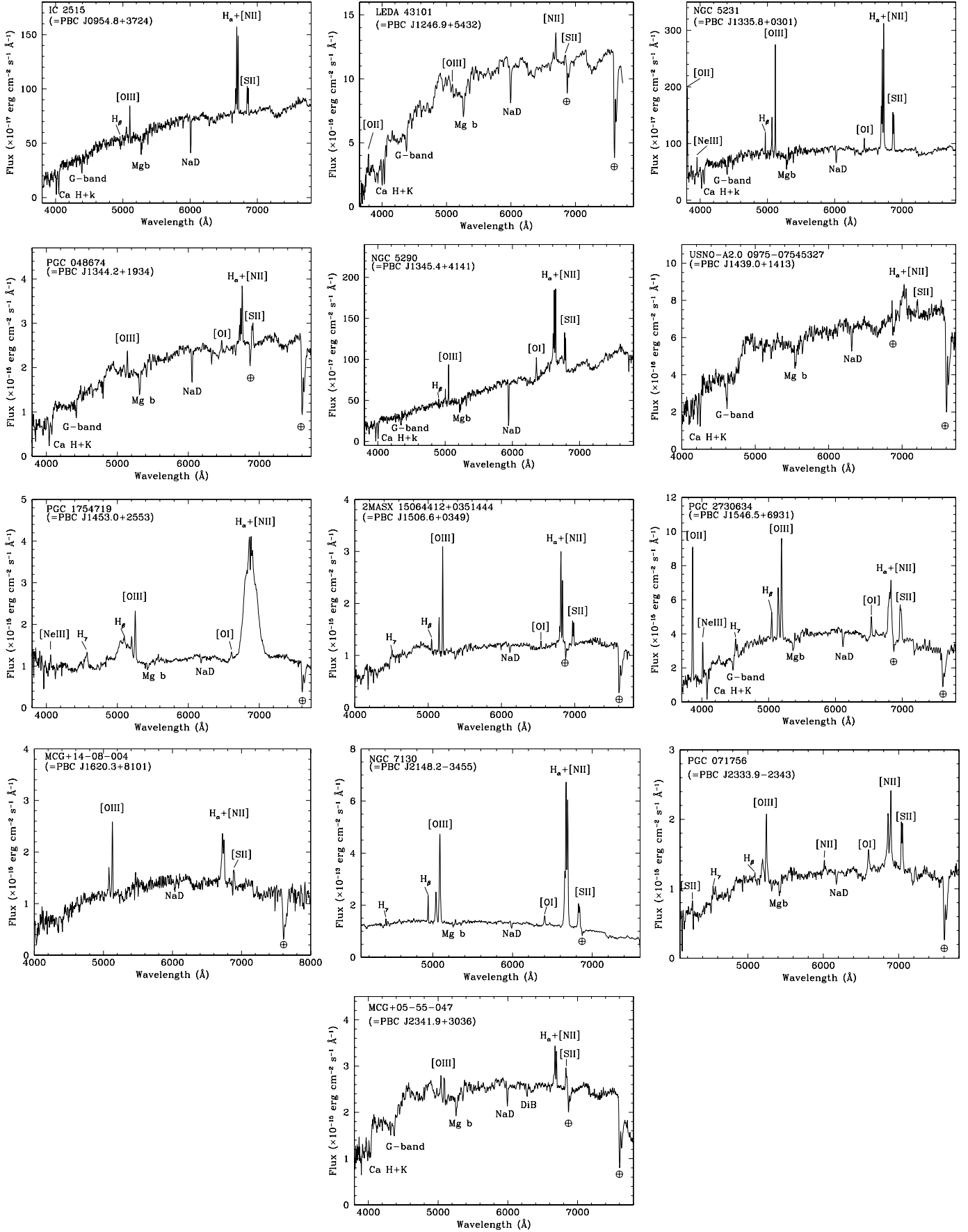


Fig. 3. Spectra (not corrected for the intervening galactic absorption) of the optical counterpart of PBC J0954.8+3724, PBC J1246.5+5432, PBC J1335.8+0301, PBC J1344.2+1934, PBC J1345.4+4141, PBC J1439.0+1413, PBC J1453.0+2553, PBC J1506.6+0349, PBC J1546.5+6931, PBC J1620.3+8101, PBC J2148.2–3455, PBC J2333.9–2343 and PBC J2341.9+3036.

from low-resolution optical spectra for the first time (see Figs. 2 and 3). Redshifts values are in the range 0.008–0.075, which means that our sources are all located in the local Universe.

All redshifts were estimated using the [OIII] narrow emission line and when this line was unavailable, from either the forbidden narrow emission lines or absorption features.

4.2.2. Optical class

For the first time, we also provide the classification of 15 sources in the sample. For the remaining 14 objects, our results only partially (50%) agree with the classifications listed in the literature.

For 5 objects (PBC J0100.6-4752, PBC J0356.9-4040, PBC 0503.0+2300, PBC 0814.4+0421, and PBC J1335.8+0301) we find a different AGN type from the one already reported. The change differs slightly for the first two sources that are now classified as Seyfert 2 galaxies rather than Seyfert 1.8–1.9 (Baumgartner et al. 2008; Winter et al. 2009); the issue is instead more important for the remaining 3 objects. PBC 0503.0+2300 and PBC 0814.4+0421 move from a Seyfert 1 classification (Cusumano et al. 2010a) to a Seyfert 1.5 and to a narrow line Seyfert 1 (NLS1), respectively. PBC J1335.8+0301 shifts from a type 1 (V&V13) to a type 2 class.

PBC J2148.2-3455 (also named NGC 7130 or IC 5135) is a known AGN, but with multiple classifications. Phillips et al. (1983), Heisler et al. (1997), and Vaceli et al. (1997) classified it as a Seyfert 2 galaxy, Thuan (1984) and Veilleux et al. (1997) assigned it a LINER type, while NED and V&V13 list it as a Seyfert 1.9. We confirm the Seyfert 2 nature of PBC J2148.2-3455 and suggest that the differences in the optical classification may simply reflect the different contributions from the starburst emission in the observations.

Baldwin et al. (1981) classified PBC J2333.9-2343 (also PKS 2331-240) as a Seyfert 2 galaxy, Radovich & Kraus (1971) instead reported it as a narrow-line radio galaxy, and Andrew et al. (1971) classed it as a quasi-stellar object, but with no redshift. Bolton (1975) defined the object morphology as an elliptical galaxy; as a result, NED classified it as a Seyfert of unclear type. We were finally able to classify the object as a Seyfert 2, thus confirming the original classification.

4.2.3. Peculiar sources and discussion

Within the sample of type 1 AGNs listed in Table 6, we find that one is a Seyfert 1, five are AGNs of intermediate type (1.2–1.9), and one is a NLS1.

In terms of the unified model, intermediate Seyferts have been interpreted as objects in which our line of sight progressively intercepts the obscuring torus starting from its outer edge. However, this is not the only possible interpretation as intermediate classifications may be related to other phenomena, such as an intrinsically variable ionizing continuum. For example, a source that would normally appear as a Seyfert 1 can be classified as an intermediate-type AGN when found in a low flux state (Trippe et al. 2010). Insights into the properties of our intermediate Seyferts can help in discriminating between the various scenarios (see next section).

PBC J0814.4+0421 deserves a special mention among type 1 AGN. LEDA 023094, which is its optical counterpart with magnitude $B = 15.5$ and redshift of 0.027, displays optical features typical of NLS1 (see Sect. 3). These sources are rare among hard X-ray selected objects since their fraction is

only 5% of all AGN and 10% of type 1 Seyferts (Panessa et al. 2011). A possible interpretation of the peculiar observational properties of NLS1 is that these systems are accreting close to their Eddington limit, implying that, compared to typical Seyfert 1 galaxies, they should host black holes with lower masses ($M_{\text{BH}} \leq 10^7 M_{\odot}$). PBC J0814.4+0421 indeed has the lowest black hole mass among the four objects for which this parameter has been estimated in this work; the value obtained is also compatible with those of other hard X-ray selected NLS1 (Panessa et al. 2011). Interestingly, PBC J1453.0+2553, the only object classified as a pure Seyfert 1 has by far the highest black hole mass observed among our small sample of type 1 AGN.

A large fraction of our extragalactic objects belong to the type 2 AGN class; this is not unexpected, as hard X-ray surveys are very efficient in discovering this type of galaxies. Among type 2 AGNs, there are also a few interesting cases, such as LINERs.

PBC J0041.6+2534 and PBC J1344.2+1934, for example, are located in an intermediate region between Seyfert 2's and LINERs in the diagnostic diagrams (Ho et al. 1993; Kauffmann et al. 2003); because of this proximity to Seyfert 2 galaxies, both are treated here as type 2 AGNs. PBC J0353.5+3713 is instead a pure LINER, but since it displays only narrow emission lines in the optical spectrum it is also considered as a type 2 AGN. Interestingly, all three objects with LINER signatures are absorbed in X-rays, thus confirming their similarity with type 2 AGN.

As a final remark, we note that all our AGN have X-ray spectra typical of their class; that is, a simple power law (either intrinsically absorbed or not) plus in many cases an extra soft component that can be parameterized by either a second power law (having the same photon index as the primary component) or a black body model. In only 3 objects do we detect emission lines compatible with neutral (in two cases) and ionized (only in one case) iron¹⁰. We do not comment on these spectra further, but we use the information on the intrinsic column density to compare in the following sections the optical versus X-ray classification and discuss the optical (dust) versus X-ray (gas) absorption.

5. X-ray versus optical classification and absorption

The unification scheme states that every AGN is intrinsically the same object, namely an accreting supermassive black hole surrounded by an obscuring torus. Depending on how the observer views the central engine, an AGN will be classified as either type 1 (where we see directly into the nucleus, hence both the broad and narrow line regions are visible) or type 2 (where we see the nucleus through the torus, which hides the BLR but not the narrow line one). Because the torus consists of dust and gas, we expect type 2 AGN to be absorbed in X-rays and optical wavelengths and type 1 not to be. The X-ray absorption is directly measured by the X-ray column density, while the optical one is estimated by means of the colour excess.

We note however that, sometimes, heavily absorbed objects also known as Compton thick AGN, appear “unabsorbed” in X-rays owing to the low statistical quality of the X-ray data and/or the lack of high energy information. To recognize these objects, we can use the diagnostic diagram of Malizia et al. (2007), which plots the X-ray absorption as a function of the source flux ratio $F_{(2-10) \text{ keV}}/F_{(20-100) \text{ keV}}$.

¹⁰ Because of the XRT sensibility, we cannot reach the 6–7 keV energy to detect the iron features in all data.

For our sample, this is done in Fig. 4, where N_{H} is for most objects the measured intrinsic absorption (see Table 3) and, for sources PBC J1453.0+2553, PBC J2148.2–3455, and PBC J2333.9–2343, the Galactic one, which is taken here as an upper limit to the X-ray absorption. A clear trend of decreasing flux ratios as the absorption increases is expected and is caused by the 2–10 keV flux being progressively depressed as the absorption becomes stronger. The two lines shown in the figure indeed describe how the flux ratio is expected to change as a function of N_{H} in the case of objects characterized by an absorbed power law having a photon index of 1.5 and 1.9, respectively. It is evident that most of our sources follow the expected trend with the most absorbed AGN showing progressively smaller $F_{(2-10)\text{ keV}}/F_{(20-100)\text{ keV}}$ values. Assuming as a dividing line between absorbed and unabsorbed AGN a column density of 10^{22} cm^{-2} (which is sufficient to hide the BLR of an active nucleus), we note that most of our AGN are above this line or very close to it, as expected given the high percentage of type 2 AGN in our sample. Indeed PBC J0503+2300 and PBC J1453.0+2553, a type 1.5 and a type 1 Seyfert respectively, are both well below the line, while 2 out of 3 Seyfert 1.9 galaxies in our sample have a column density above 10^{22} cm^{-2} , i.e. compatible with the idea that these objects are observed through the edge of the torus; the third one, PBC J1546.5+6931, has a column density just below the dividing line between absorbed and unabsorbed objects.

PBC J0814.4+0421, the only NLS1 in the sample, is absorbed, although this is not unusual, as the presence of strong, partial, and/or stratified absorption is one of the two competing models used to explain the complex X-ray spectra of this class of AGN (Panessa et al. 2011).

The only type 1 AGN for which absorption is totally unexpected is PBC J0543.6-2738, which is classified as a type 1.2 AGN, but displays a column density in the range $(1.4-5.5) \times 10^{22}\text{ cm}^{-2}$; it is possible that in this source the gas responsible for the X-ray absorption is highly ionized, instead of being neutral, in which case the accompanying dust would sublimate, yielding a much smaller dust-to-gas ratio and resulting in a reduced optical extinction and consequently in an early type 1 classification. From this perspective, the obscuring material would not be related to the toroidal structure as assumed in the unified theory, but rather to other types of absorption, possibly gas in an outflow from the central nucleus (Winter et al. 2011). Unfortunately, our X-ray spectrum does not have a S/N high enough to enable us to distinguish between ionized and neutral gas models; clearly PBC J0543.6-2738 merits a far more in-depth X-ray study with satellites such as *XMM-Newton* or *Suzaku*.

On the other hand, we find two objects that are classified as type 2 Seyferts in optical, but show no absorption in X-rays: PBC J2148.2–3455 and PBC J2333.9-2343. As anticipated above, it is possible that these 2 AGN are Compton thick sources not recognized as such owing to the low quality of the X-ray data; but while this may be the case for the first source, it is certainly not true for the second one, for the following reasons.

PBC J2148.2–3455 is well-studied in X-rays and previous observations strongly indicate that this is indeed a Compton thick AGN. Using Chandra data, Levenson et al. (2005) showed that the active nucleus is probably buried beneath a column density $N_{\text{Hx}} \geq 10^{24}\text{ cm}^{-2}$ as indicated by the prominent Fe $K\alpha$ emission line, which has an equivalent width larger than 1 keV; in addition the $F_{2-10}\text{ keV}/F[\text{OIII}]$ ratio, which is often used as an alternative way of pinpointing heavily absorbed Seyfert 2 galaxies, is sufficiently small (0.04) to classify the source as

a Compton thick object (Bassani et al. 1999). On the other hand, PBC J2333.9-2343, is quite atypical: it lies in the region of type 1 AGN (see Fig. 4, top panel), has a good quality spectrum that provides no indication of an iron line and has a $F_{2-10}\text{ keV}/F[\text{OIII}]$ ratio of ~ 1 , again similar to type 1 Seyferts (Bassani et al. 1999). The source is peculiar in many other ways: it is listed in the Roma BZCAT as a blazar of unknown type (Massaro et al. 2009), is a flat spectrum radio source (Healey et al. 2007), shows a jet feature in a VLBI 8.4 GHz image, is variable in radio (Ojha et al. 2004), and in X-rays according to a quick look analysis of all publicly available *Swift*/XRT observations and is finally polarized at radio frequencies (Ricci et al. 2004). This source resembles a nearby blazar, but it has the optical spectral appearance of a type 2 Seyfert, which is quite unusual since flat spectrum radio quasars (one of two types of blazars) are generally broad-line AGN. This is an object that certainly deserves further investigation in X-rays, but also in other wavebands to confirm the above peculiarities.

Summarizing, we find that the optical versus X-ray classifications for most of our sources broadly fit with the AGN unified scheme, except for a few peculiar objects: PBC J0543.6-2738, which is a type 1 AGN showing some absorption possibly due to outflowing gas, and PBC J2333.9-2343, which is instead a type 2 AGN displaying no absorption and with properties similar to blazars.

In Fig. 4 bottom panel, we plot the X-ray column density versus the optical one (with relative uncertainties), which was measured from the intrinsic colour index $E(B-V)$ using the formula $N_{\text{Hopt}} = 3.1 E(B-V) \times 1.79 \times 10^{21}\text{ cm}^{-2}$ (Predehl & Schmitt 1995; Rieke & Lebofski 1985). For 5 sources, we decided to take 90% upper limits (marked with red arrows, in Fig. 4) because the errors were larger than the N_{Hopt} values. Within the unified theory, the X-ray absorption associated with the gas in the torus, which is confined to a region smaller than the narrow line region (NLR); the optical extinction, on the other hand, may come from dust either associated with the torus (internal reddening) or to larger-scale structures such as lanes, bars, or something else (external reddening). As clear from the figure, the majority of our sources has an X-ray column density higher than the optical one. Since most of our objects are AGN of type 2, the optical reddening is related to the NLR, hence is most likely associated with internal rather than external reddening, i.e. the torus; in this case, the bottom panel in Fig. 4 is simply telling us that, with this structure, gas absorption is greater than dust obscuration. This effect was already noticed by Maiolino et al. (2001), who suggested that in AGN the dust-to-gas ratio is much lower than the galactic one or that in the inner parts of the obscuring torus the dust is sublimated by the strong UV radiation field. Another interesting possibility put forward by the same authors is that the dust extinction curve is much flatter than the standard galactic one, for example as a result of the growth of larger dust grains. Only 3 of our objects are located above the 1–1 line implying that there is an optical/(dust) extinction similar to or slightly higher than the X-ray/(gas) absorption. Two of these objects are type 1 AGN and so this is to be expected, as our line of sight to their central nucleus does not intercept the torus; the third object is PBC J1345.4+4141, which is the only type 1.9 AGN of our sample that has an X-ray column density close to but lower than 10^{22} cm^{-2} . In this case, it is possible that the optical reddening and the X-ray absorption are unrelated to the torus, but may come from other larger-scale structures. We note that NGC 5290, the optical counterpart of PBC J1345.4+4141, forms a pair of interacting galaxies with NGC 5289 (van Driel et al. 2001); the latter also shows a bright

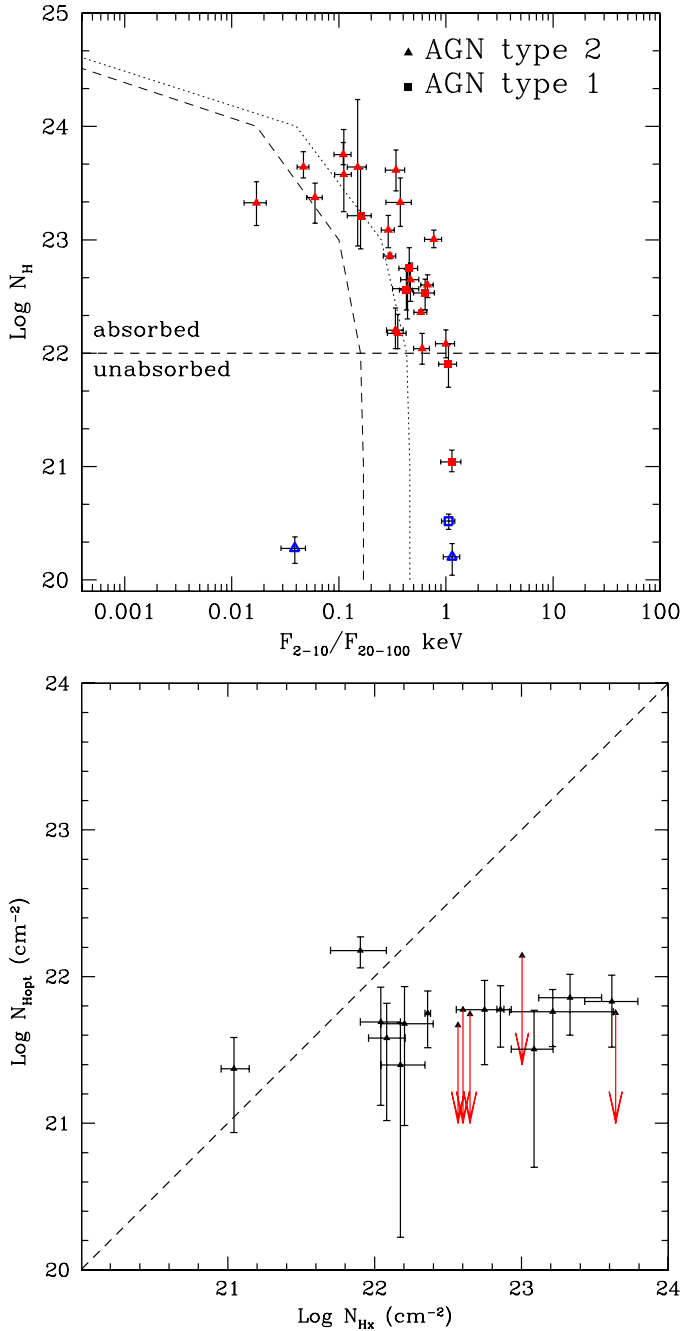


Fig. 4. *Top panel:* $F_{2-10 \text{ keV}}/F_{20-100 \text{ keV}}$ flux ratio of our sample. Lines correspond to expected values for an absorbed power-law with photon index 1.5 (dotted) and 1.9 (dashed); see text for details. The blue empty symbols indicate sources with Galactic absorption only, while red-filled ones correspond to sources with an extra intrinsic absorption. *Bottom panel:* X-ray column density versus the optical one computed from the $E(B - V)$ assuming the Galactic extinction law of Cardelli et al. (1989). Triangles are Seyfert 2, squares are Seyfert 1 objects. Points marked with red arrows are upper limits.

bulge, which is partially hidden by a dark lane and asymmetric absorption (see NED notes). In other words, there is plenty of reddening on large scales to explain the observed properties. It is also possible that in this source the BLR optical continuum has temporarily diminished, leaving visible only a very weak broad $\text{H}\beta$ line and leading to the classification as a type 1.9, even if the nucleus is totally unobscured by dust (and also by gas given the not-so-high column density). This is another object for which

further observations are clearly encouraged especially at optical/infrared wavelengths.

6. Conclusions

We have either provided for the first time, confirmed, or corrected the optical spectroscopic identifications of 29 sources belonging to the Palermo 39 month *Swift* /BAT catalogue (Cusumano et al. 2010a). This has been achieved by performing a multisite observational campaign in Europe, South Africa, and Central America.

We have found that our sample is composed of 28 AGN (7 of type 1 and 21 of type 2), with redshifts between 0.008 and 0.075, and 1 CV. Among the extragalactic sources, we found some peculiar objects, such as 3 AGN showing LINER features and 1 object with the properties of a NLS1. For 4 type 1 AGN, we have estimated the BLR size, velocity, and the central black hole mass. We have performed an X-ray spectral analysis of the entire sample and found that overall our sources display X-ray spectra typical of their optical class. More specifically, we have compared the optical to X-ray classifications of our galaxies, to test the AGN unified theory. We found a generally good match between optical class and X-ray absorption, thus validating the unified scheme. However, in a few sources there is a clear discrepancy between the optical and X-ray classifications: PBC J0543.6-2738 is a Seyfert 1.2 displaying mild X-ray absorption, possibly owing to outflowing gas; PBC J1345.4+4141 is instead a Seyfert 1.9 showing no absorption, although its optical class may be related to reddening occurring in large-scale structures or due to a low optical ionization state. More convincingly, outside the unified scheme is PBC J2333.9-2343, which is a Seyfert 2 without an intrinsic X-ray column density; this source has many features that make it very similar to broad-line blazars and yet has only narrow lines in its optical spectrum. Another Seyfert 2 displaying no absorption is PBC J2148.2-3455, but through the use of our diagnostic diagram and information gathered in the literature we conclude that this source is either a Compton thick or heavily absorbed AGN, which is therefore compatible with its optical class. We also compared the X-ray gas absorption with the optical dust reddening for the AGN sample: we find that for most of our sources, specifically those of type 1.9–2, the former is higher than the latter, confirming the early results of Maiolino et al. (2001); this is possibly due to the properties of dust in the circumnuclear obscuring torus of the AGN.

As a final remark, we stress the importance of combining optical with X-ray spectroscopy for hard X-ray selected objects: using information in both wavebands enables us to increase the number of source identifications and classifications, but also perform statistically significant population studies, to understand the physical processes occurring in these objects and study the AGN unified model.

Acknowledgements. We thank Dr. Domitilla de Martino for useful discussions and the referee for comments that helped us to improve the quality of this paper. We also thank Silvia Galletti for Service Mode observations at the Loiano telescope, and both Antonio De Blasi and Ivan Bruni for night assistance at the Loiano telescope. We also thanks Claudia Reyes for night assistance at the ESO NTT telescope. This work is based on observations obtained with *XMM-Newton*, an ESA science mission with instruments and contributions directly funded by ESA Member States and NASA. We also acknowledge the use of public data from the *Swift* data archive. This research has made use of the ASI Science Data Center Multimission Archive, of the NASA Astrophysics Data System Abstract Service, the NASA/IPAC Extragalactic Database (NED), of the NASA/IPAC Infrared Science Archive, which are operated by the Jet Propulsion Laboratory, California Institute of Technology, under contract with the National Aeronautics and Space Administration and of

data obtained from the High Energy Astrophysics Science Archive Research Center (HEASARC), provided by NASA's GSFC. This publication made use of data products from the Two Micron All Sky Survey (2MASS), which is a joint project of the University of Massachusetts and the Infrared Processing and Analysis Center/California Institute of Technology, funded by the National Aeronautics and Space Administration and the National Science Foundation. This research has also made use of data extracted from the 6dF Galaxy Survey and the Sloan Digitized Sky Survey archives; the SIMBAD database operated at CDS, Strasbourg, France, and of the HyperLeda catalogue operated at the Observatoire de Lyon, France. The authors acknowledge the ASI and INAF financial support via grants Nos. I/033/10/0, I/009/10/0; P.P. is supported by the INTEGRAL ASI-INAF grant No. 033/1070. L.M. is supported by the University of Padua through grant No. CPDR061795/06. G.G. is supported by FONDECYT 1085267. V.C. is supported by the CONACyT research grants 54480 and 15149 (México). D.M. is supported by the Basal CATA PFB 06/09, and FONDAP Center for Astrophysics grant No. 15010003.

References

- Adelman-McCarthy, J. K., Agüeros, M. A., Allam, S. S., et al. 2007, *ApJS*, 172, 634
- Andrew, B. H., Harvey, G. A., Medd, W. J. 1971, *ApL*, 9, 151
- Baldwin, J. A., Wampler, E. J., Burbidge, E. M. 1981, *ApJ*, 243, 76
- Barthelmy, S. D. 2004, *Proc. SPIE*, 5165, 175
- Bassani, L., Dadina, M., Maiolino, R., et al. 1999, *ApJS*, 121, 473
- Baumgartner, W. H., Tueller, J., Mushotzky, R. F., et al. 2008, *ATel*, 1794
- Bolton, J. G., Shimmins, A. J., & Wall, J. V. 1975, *AuJPA*, 34, 1
- Burrows, D. N., Hill, J. E., Nousek, J. A., et al. 2004, *Proc. SPIE*, 5165, 201
- Cardelli, J. A., Clayton, G. C., & Mathis, J. S. 1989, *ApJ*, 345, 245
- Ciroi, S., Di Mille, F., Zaccaria, M., et al. 2009, *Atel*, 1985
- Cusumano, G., La Paola, V., Segreto, A., et al. 2010a, *A&A*, 510, A48
- Cusumano, G., La Paola, V., Segreto, A., et al. 2010b, *A&A*, 524, A64
- Dickey, J. M., & Lockman, F. J. 1990, *ARA&A*, 28, 215
- Doyle, M. T., Drinkwater, M. J., Rohde, D. J., et al. 2005, *MNRAS*, 361, 34
- Gehrels, N., Chincarini, G., Giommi, P., et al. 2004, *ApJ*, 611, 1005
- González-Martín, O., Masegosa, J., Marquez, I., et al. 2009, *ApJ*, 704, 1570
- Healey, S. E., Romani, R. W., Taylor, G. B., et al. 2007, *ApJS*, 171, 61
- Heckman, T. M. 1980, *A&A*, 87, 152
- Heisler, C. A., Lumsden, S. L., & Bailey, J. A. 1997, *Nature*, 385, 700
- Hill, J. E., Burrows, D. N., Nousek, J. A., et al. 2004, *Proc. SPIE*, 5165, 217
- Ho, L. C., Filippenko, A. V., & Sargent, W. L. W. 1993, *ApJ*, 417, 63
- Ho, L. C., Filippenko, A. V., & Sargent, W. L. W. 1997, *ApJS*, 112, 315
- Horne, K. 1986, *PASP*, 98, 609
- Jones, D. H., Saunders, W., Colless, M., et al. 2004, *MNRAS*, 355, 747
- Jones, D. H., Saunders, W., Read, M., & Colless, M. 2005, *PASA*, 22, 277
- Kaspi, S., Smith, P. S., Netzer, H., et al. 2000, *ApJ*, 533, 631
- Kauffmann, G., Heckman, T. M., Tremonti, C., et al. 2003, *MNRAS*, 346, 1055
- Landi, R., Bassani, L., Dean, A. J., et al. 2009, *MNRAS*, 392, 630
- Levenson, N. A., Weaver, K. A., Heckman, T. M., et al. 2005, *ApJ*, 618, 167
- Maiolino, R., Marconi, A., Salvati, M., et al. 2001, *A&A*, 365, 28
- Malizia, A., Landi, R., Bassani, L., et al. 2007, *ApJ*, 668, 81
- Masetti, N., Palazzi, E., Bassani, L., et al. 2004, *A&A*, 426, L41
- Masetti, N., Bassani, L., Bazzano, A., et al. 2006a, *A&A*, 455, 11
- Masetti, N., Morelli, L., Palazzi, E., et al. 2006b, *A&A*, 459, 21
- Masetti, N., Mason, E., Morelli, L., et al. 2008, *A&A*, 482, 113
- Masetti, N., Parisi, P., Palazzi, E., et al. 2009, *A&A*, 495, 121
- Masetti, N., Parisi, P., Palazzi, E., et al. 2010, *A&A*, 519, A96
- Masetti, N., Parisi, P., Jiménez-Bailón, E., et al. 2012, *A&A*, 538, A123
- Massaro, E., Giommi, P., Leto, C., et al. 2009, *A&A*, 495, 691
- Monet, D. G., Levine, S. E., Canzian, B., et al. 2003, *AJ*, 125, 984
- Moretti, A., Campana, S., Tagliaferri, G., et al. 2004, *SPIE Proc.*, 5165, 232
- Mushotzky, R. F., Done, C., & Pounds, K. A. 1993, *ARA&A*, 31, 717
- Noguchi, K., Terashima Y., & Awaki, H. 2009, *ApJ*, 705, 454
- Ojha, R., Fey, A. L., Johnston, K. J., et al. 2004, *AJ*, 127, 3609
- Osterbrock, D. E. 1989, *Astrophysics of Gaseous Nebulae and Active Galactic Nuclei* (Mill Valley: Univ. Science Books)
- Osterbrock, D. E., & Pogge, R. W. 1985, *ApJ*, 297, 166
- Panessa, F., de Rosa, A., Bassani, L., et al. 2011, *MNRAS*, 417, 2426
- Parisi, P., Masetti, N., Jiménez-Bailón, E., et al. 2009, *A&A*, 507, 1345
- Patterson, J., & Raymond, J. C. 1985, *ApJ*, 292, 535
- Phillips, M. M., Charles, P. A., & Baldwin, J. A. 1983, *ApJ*, 266, 485
- Predehl, P., & Schmitt, J. H. M. M. 1995, *A&A*, 293, 889
- Prugniel, P. 2005, *The Hyperleda Catalogue*, <http://leda.univ-lyon1.fr/>
- Radovich, M. M., & Kraus, J. D. 1971, *AJ*, 76, 683
- Ricci, R., Prandoni, I., Gruppioni, C., et al. 2004, *A&A*, 415, 549
- Rieke, G. H., & Lebofsky, M. J. 1985, *ApJ*, 288, 618
- Schlegel, D. J., Finkbeiner, D. P., & Davis, M. 1998, *ApJ*, 500, 525
- Skrutskie, M. F., Cutri, R. M., Stiening, R., et al. 2006, *AJ*, 131, 1163
- Strüder, L., Briel, U., Dennerl, K., et al. 2001, *A&A*, 365, L18
- Thuan, T. X. 1984, *ApJ*, 281, 126
- Trippe, M. L., Crenshaw, D. M., Deo, R. P., et al. 2010, *ApJ*, 725, 1749
- Ubertini, P., Lebrun, F., Di Cocco, G., et al. 2003, *A&A*, 411, L131
- Vaceli, M. S., Viegas, S. M., Gruenwald, R., et al. 1997, *AJ*, 114, 1345
- van Driel, W., Marcum, P., Gallagher, J. S., et al. 2001, *A&A*, 378, 370
- Veilleux, S., & Osterbrock, D. E. 1987, *ApJS*, 63, 295
- Veilleux, S., Godrich, R. W., & Hill, G. J. 1997, *ApJ*, 477, 631
- Veron-Cetty, M. P., & Veron, P. 2010, *A&A*, 518, A10
- Voges, W., Aschenbach, B., Boller, T., et al. 1999, *A&A*, 349, 389
- Warner, B. 1995, *Cataclysmic variable stars* (Cambridge: Cambridge University Press)
- Watson, M. G., Schröder, A. C., Fyfe, D., et al. 2009, *A&A*, 493, 339
- Winkler, H. 1992, *MNRAS*, 257, 677
- Winkler, C., Courvoisier, T. J.-L., Di Cocco, G., et al. 2003, *A&A*, 411, L1
- Winter, L. M., & Taylor, T. 2011, *BAAS*, 21732606W
- Winter, L. M., Mushotzky, R. F., Reynolds, C. S., et al. 2009, *ApJ*, 690, 1322
- Wright, E. L. 2006, *PASP*, 118, 1711
- Wu, X.-B., Wang, R., Kong, M. Z., Liu, F. K., & Han, J. L. 2004, *A&A*, 424, 793